DOI: 10.13009/EUCASS2019-123

Drag reduction control in turbulent channel using spanwise traveling wave of blowing and suction methods

Yi Huang[1] and Song Fu[2]

[1] Tsinghua University, Beijing 100080, China,
[2] Tsinghua University, Beijing 100080, China,
fs-dem@tsinghua.edu.cn

Abstract. The drag reduction control strategy, spanwise traveling wave of wall blowing and suction, is investigated in turbulent channel flow with $Re_\tau = 180$. With proper parameters, the drag reduction can reach 2% now. The mechanism behind this we conclude is that the spanwise traveling wave can weaken the normal streamwise stress and shear stress. And the burst and sweep events of the streamwise vortex are weakened in some extent because of the non-uniformed blowing and suction in spanwise direction. The linearized fluctuation equations show that the wall blowing and suction form drag reduction and increase regions, and the traveling wave makes the whole effect a drag reduction.

Keywords: spanwise traveling wave, drag reduction, turbulent channel flow

1 Introduction

Drag reduction control is an important part in flow control field since there are about 60% of the total drag is the viscous drag for a Boeing aircraft. As for the energy consumption, 1% drag reduction in viscous drag will lead to 0.75% reduction in fuel consumption . For the energy input aspect, the control strategies can be separated to 2 categories, passive control and active control. For passive control, there is no extra energy input. For example, building riblets at the wall can achieve a drag reduction about 10%[1], by limiting the spanwise motion of the near wall streaks. For active control, extra energy is needed and it usually has larger drag reduction efficiency compared to passive control. Among the active control methods, the direction of the actuation could be spanwise(Sp-) and wall normal(Wn-). In addition, the fluctuaions can be uniform in some direction(U-uniform), or a traveling wave form (TW-traveling wave).Quadrio et al [2][3][4]have done lots of simulations investigating the active control, spanwise actuation, which is called wall oscillation. The wall oscillation can be uniform, or a traveling wave in streamwise direction (Sp-StTW) or spanwise direction (Sp-SpTW). According to their articles, this control strategy could lead to a drag reduction about 40% by inclining the streamwise vortex to spanwise direction.

DOI: 10.13009/EUCASS2019-123

Min et al [5]proposed a control strategy to generate wall normal actuation by blowing and suction at the wall. Min proposed the streamwise traveling wave of wall blowing and suction (StTW-v)control in turbulent channel, which can reduce the drag even to the corresponding laminar level when the traveling direction of the wave is opposite to the main flow direction. The traveling wave of blowing and suction will induce a flux opposite to the wave traveling direction, which decrease the pressure drop needed in the channel then leads to a drag reduction. Fukagata et al [6] also proposed the wall deformation forming a traveling wave in spanwise direction(SpTW-y), which has a drag reduction about 10%. The quasi-streamwise vortex are shielded from the wall by the spanwise motion induced by the wall motion.

Based on the previous work, we investigate the drag reduction efficiency of the active control, which is wall normal actuation forming a traveling wave in spanwise direction. Different from the wall deformation actuation from Fukagata, the wall blowing and suction actuation is used here in our study, which we call spanwise traveling wave of wall blowing and suction control (Wnbs-SpTW, or SpTW-v). This control method can achieve about 2% reducion in drag now. When the direction of wave propagation is alternated with time, which is similar to the wall oscillation, we can achieve a higher drag reduction about 30%.

The structure of following sections: the second section shows the numerical method, channel flow base-flow and induced flow by the active control; the third section analyzes the mechanism of the drag reduction; the forth section introduces the modified actuation with alternated wave propagation direction and the last section summarizes and gets a conclusion.

2 Numerical Method

In this section, we will show the numerical method in this article and the base flow to control. We use the numerical method based on the high accuracy flux reconstruction method, FR or CPR (Correction Procedure via Reconstruction, CPR)[7] in the whole work. This numerical scheme is one of the discrete finite element method, similar to the discontinuous Galerkin method. For a hyperbolic conservation equation:

$$\frac{\partial Q}{\partial t} + \overrightarrow{\nabla} \cdot \overrightarrow{F}(Q) = 0 \tag{1}$$

with proper initial and boundary condition, where Q is the state vector and $\overrightarrow{F} = (F, G)$ is the flux vector. For the computational domain discretized by non-staggered grids $V_i, i = 1, ..., N$, the equations can be expressed equally within an arbitrary element V_i:

$$\int_{V_i} (\frac{\partial Q}{\partial t} + \overrightarrow{\nabla} \cdot \overrightarrow{F}(Q)) W dV = 0 \tag{2}$$

where W is a weight function. Using the Stokes integration theorem, the equation(2) can be rearranged as:

$$\int_{V_i} \frac{\partial Q}{\partial t} W dV + \int_{\partial V_i} W \overrightarrow{F}(Q) \cdot \overrightarrow{n} dS - \int_{V_i} \overrightarrow{\nabla} W \cdot \overrightarrow{F}(Q) dV = 0 \tag{3}$$

DOI: 10.13009/EUCASS2019-123

where ∂V_i means the boundary of the element V_i. Since the solution at the interface is discontinuous, the normal flux term is replaced with a common Riemann flux similar to the Godunov method:

$$\overrightarrow{F}(Q) \cdot \overrightarrow{n} = F^n(Q) \approx F^n_{com}(Q_{left}, Q_{right}, \overrightarrow{n}) \tag{4}$$

where the Q_{left}, Q_{right} represent the value of Q computed at left element and right element of the interface. Use the integration by parts to the last term in the right hand term in equation (3):

$$\int_{V_i} \frac{\partial Q}{\partial t} W dV + \int_{\partial V_i} W[F^n_{com} - F^n(Q)]dS - \int_{V_i} W \overrightarrow{\nabla} \cdot \overrightarrow{F}(Q) dV = 0 \tag{5}$$

Introduce a "correction field" on V_i, δ_i is a polynomial on element V_i with an order k, such that:

$$\int_{V_i} W \delta_i dV = \int_{\partial V_i} W[F^n] dS \tag{6}$$

where $[F^n] = F^n_{com} - F^n(Q)$ is the normal flux difference. The equation (6) is always referred to as the "lifting operator", which get a polynomial δ_i from the normal flux difference at the interface. Then we obtain:

$$\int_{V_i} (\frac{\partial Q}{\partial t} + \overrightarrow{\nabla} \cdot \overrightarrow{F}(Q) + \delta_i) W dV = 0 \tag{7}$$

Since the flux term $\overrightarrow{F}(Q)$ is not a linear function of Q, it need projecting to the $k-$order polynomial test space on element V_i, and then we obtain from (7)

$$\frac{\partial Q}{\partial t} + \Pi(\overrightarrow{\nabla} \cdot \overrightarrow{F}(Q)) + \delta_i = 0 \tag{8}$$

where Π is the projection function. As mentioned above, the solution points are chose as the Guass integration points in each element and the discrete equations we solve finally is:

$$\frac{\partial Q_j}{\partial t} + \Pi_j(\overrightarrow{\nabla} \cdot \overrightarrow{F}(Q)) + \delta_{i,j} = 0 \tag{9}$$

where j is the index of the solution point. The lifting operator can be computed from equation (6):

$$\delta_{i,j} = \frac{1}{|V_i|} \sum_{f,m} \alpha_{j,f,m} [F^n_{f,m}] S_f \tag{10}$$

where f is the index of the interface, and m means the index of the flux point in the face, and α is the coefficients. This lifting operator is only dependent on the geometry and the weight function of the element. Details of the methods are referred to the articles([7]), which will not be discussed here..

As for the viscous term, we use BR2 (Bassi-Rebay) scheme. And the time evolution scheme is chose explicit 3 step Runge-Kutta method. In the present studies, 4-order interpolation is used in each element. All the numerical cases are conducted with direct numerical simulation(DNS). The flow induced by the actuation in two dimensional(2D) quiescent surroundings will be talked about below firstly.

DOI: 10.13009/EUCASS2019-123

2.1 Induced flow by the actuation

Here we use treat the actuation a velocity boundary condition at the wall, which means $v_w = V_0 \cos(k(x - ct)$ (SpTW-v, spanwise traveling wave of v velocity), where V_0, k, c represents the amplitude, wavenumber and wavespeed, repectively and $c > 0$ means the wave is traveling in $+x$ direction while $c < 0$ means in $-x$ direction. For the induced flow by the traveling wave of wall blowing and suction, two dimensional numerical computations have been done with different sets of the parameters, (V_0, k, c). The sketch of the flow is showed in Fig.1. Half-infinite in wall normal direction computational domain is considered here, for simplicity. where x, y denotes the transverse and wall normal direction. The actuation is

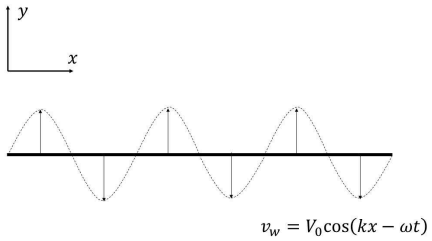

Fig. 1. The sketch of the two dimensional flow induced by the SpTW-v

imposed on the wall and above the wall is an infinite field. Now we introduce the flow induced by this actuation in this half-infinite field. The dimensionless Navier-Stokes (NS) equations in this case are(Eq.2.1,13):

$$\frac{\partial}{\partial t}u + \alpha u \cdot \nabla u = -\nabla p + \frac{1}{Re_\omega}\nabla^2 u \tag{11}$$

$$\nabla \cdot u = 0 \tag{12}$$

where the $Re_\omega = \beta = \frac{\rho\omega}{\mu k^2}$, with the boundary condition:

$$v = \begin{cases} \sin(\eta x + t), & y = 0 \\ 0, & y \to \infty \end{cases} \tag{13}$$

The variables above are non-dimensionalized by (Eq.14):

$$\hat{x} = hx, \hat{u} = V_0 u, \hat{p} = \rho\omega h V_0 p, \hat{t} = \frac{1}{\omega}t \tag{14}$$

$$\alpha = \frac{V_0}{h\omega}, Re_\omega = \beta = \frac{\rho h^2 \omega}{\mu}, Re = \frac{\rho h V_0}{\mu}, \eta = kh \tag{15}$$

This nonlinear NS equations can not be solved theoretically directly but an asymptotic solution is achieved using small parameters expansion based on α

DOI: 10.13009/EUCASS2019-123

(**??**).

$$u = u_0 + \alpha u_1 + \alpha^2 u_2 + ... \tag{16}$$
$$\Phi = \Phi_0 + \alpha \Phi_1 + \alpha^2 \Phi_2 + ... \tag{17}$$

Where Φ is the stream function. The leading order solution, or the linearized solution of the equation is as follows (Eq.18):

$$u_0(x,y,t) = \frac{1}{(1-a)^2+b^2}\{[(a-a^2-b^2)\cos(x+t) - b\sin(x+t)]e^{-y} \tag{18}$$
$$+ [(a^2-a+b^2)\cos(x+t-by) + b\sin(x+t-by)]e^{-ay}\} \tag{19}$$
$$v_0(x,y,t) = \frac{1}{(1-a)^2+b^2}\{[(a^2-a+b^2)\sin(x+t) - b\cos(x+t)]e^{-y} \tag{20}$$
$$+ [(1-a)\sin(x+t-by) + b\cos(x+t-by)]e^{-ay}\} \tag{21}$$

where $a = \sqrt{\frac{\sqrt{1+\beta^2}+1}{2}}, b = \sqrt{\frac{\sqrt{1+\beta^2}-1}{2}}$. Learning from the solution, we know the flow field is only related to one parameter β, since the length is normalized by wavelength and the time is normalized by period of the wave. There are 2 parts in the velocity equation, which are e^{-y} and e^{-ay} decay part. The former distribution is in same phase along the wall normal direction, while the laster has different phase along wall normal direction. As mentioned above,$a = \sqrt{\frac{\sqrt{1+\beta^2}+1}{2}} > 1$ is always true, which means e^{-ay} comes to zeros faster than e^{-y} part, and much faster when β is large. Here we show some flow field with different β value (Fig.2,3). Of course, the envelope of the velocity profile can be deduced as

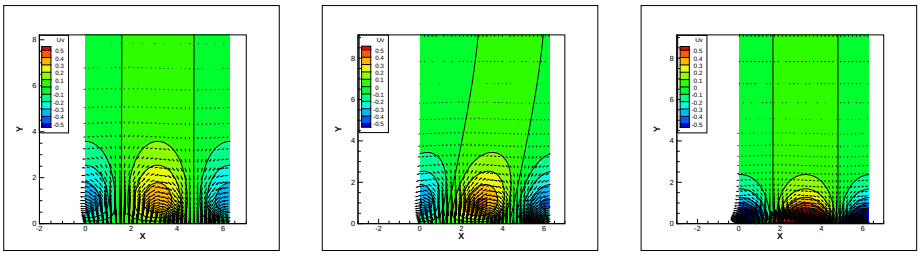

(a) $\beta = 0.01$ (b) $\beta = 1$ (c) $\beta = 100$

Fig. 2. The (u, v) vector and u contour

(Eq.22):

$$En_u(y) = \frac{\sqrt{(a^2+b^2-a)^2+b^2}}{(1-a)^2+b^2}\sqrt{e^{-2y}+e^{-2ay}-2\cos(by)e^{-(1+a)y}} \tag{22}$$

DOI: 10.13009/EUCASS2019-123

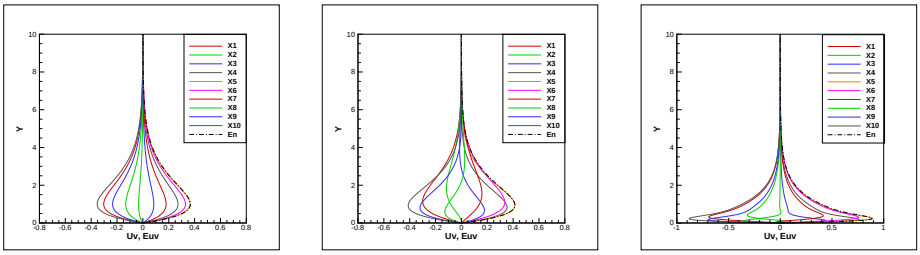

(a) $\beta = 0.01$ (b) $\beta = 1$ (c) $\beta = 100$

Fig. 3. The transverse velocity profile at 10 different location $X1, X2...X10$ and the velocity envelope

With $\beta \to 0$ and $\beta \to \infty$, the velocity is close to (Eq.23):

$$\begin{aligned} \beta \to 0 \ : u &= -y\cos(x+t)e^{-y} \\ v &= -(1+y)\sin(x+t)e^{-y} \\ \beta \to \infty : u &= -\cos(x+t)e^{-y} \\ v &= \sin(x+t)e^{-y} \end{aligned} \tag{23}$$

Here in $\beta \to \infty$ situation, the transverse velocity u doesn't satisfy the boundary condition, which we think the e^{-ay} part in Eq.18 decay much faster than the e^{-y} part, and it makes the velocity looks like in Eq.23 form. And the envelope in these 2 limitation (Eq.24):

$$\begin{aligned} \beta \to 0 \ : En_u &= ye^{-y} \\ En_v &= (1+y)e^{-y} \\ \beta \to \infty : En_u &= e^{-y} \\ En_v &= e^{-y} \end{aligned} \tag{24}$$

The envelope with different β value is showed in Fig.4 With the analysis results showed above, we got these conclusion:

1. The nondimensional velocity u, v of the flow induced by SpTW-v actuation is only related to $\beta = \frac{\rho\omega}{\mu k^2}$, where ω, k is the frequency and wavelength of the traveling wave.
2. The expression form of the velocity u, v has 2 decay part, e^{-y} and e^{-ay}, where $a = \sqrt{\frac{\sqrt{1+\beta^2}+1}{2}}$, which means e^{-ay} parts decay faster and
3. With increasing β, the maximum point of the u envelope gets closer to the wall and the maximum velocity gets larger (it can be > 1), while v envelope gets closer to e^{-y}.
4. With the envelope, we can find the height of the layer is always near the 2π range, which means it is close to the wavelength.

In fact, the actuation is imposed on both walls out of phase to maintain the symmetry of the channel, which means $v_{bottom} = -v_{top}$. The computation

DOI: 10.13009/EUCASS2019-123

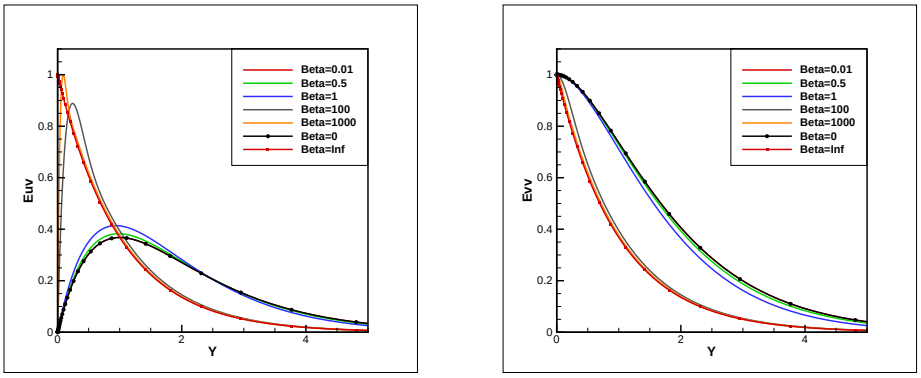

(a) u velocity (b) v velocity

Fig. 4. The envelope of the transverse velocity with different β value

domain is $L_x \times L_y = [0, 2\pi] \times [-1, 1]$ (in Fig.5)with incompressible NS equation solver. The same method can be used to solve the NS equations in this condition, and the details are referred to (**??**). Here we just show the computational results of the actuation in a channel domain. Here the viscosity is set as $\nu = 3.571428 \times$

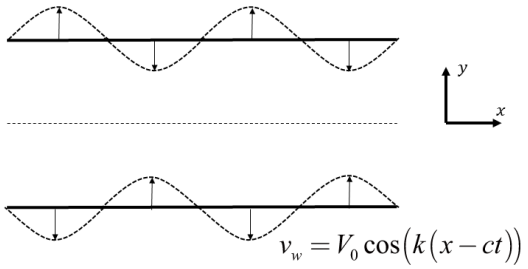

Fig. 5. The sketch of the two dimensional flow induced by the SpTW-v in channel

10^{-4}, which is the same as the one used in 3D control flow simulation. From the results of these 2D simulation and previous studies(**??**,**??**), we think the characteristics of the induced flow are (Fig.6):

1. The induced flow has two kinds of regions, forward region and backward region.(The induced backward region(surrounded by red dash line) and forward region (surrounded by blue dash line) The transverse motion in forward region coincides with the wave propagation direction and in backward region it is opposite to the wave propagation direction, as a result of the non-linear term. (in Fig.6)

DOI: 10.13009/EUCASS2019-123

2. With increasing wave speed, the forward region shrinks and the backward region extend, which leads to an opposite flux.
3. The opposite flux gets smaller with increasing wavespeed when the wavespeed is high enough.

The same method can be used to solve the NS equations in this condition, and the details are referred to (**??**)

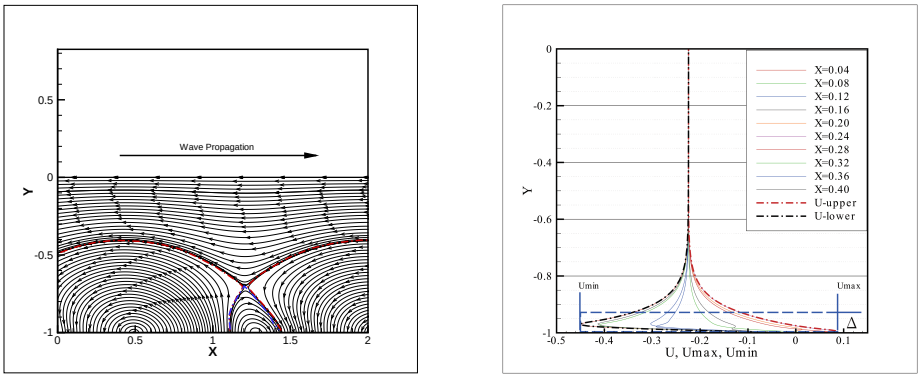

(a) Streamline (b) u velocity profile

Fig. 6. The transverse velocity profile and streamline with $(V_0, k, c) = (0.3, 16, 1.0)$

DOI: 10.13009/EUCASS2019-123

2.2 Uncontrolled Flow

The base flow used for control is the fully developed turbulent channel flow with $Re_\tau = u_\tau h/\nu = 180 (Re_b = \rho U_b h/\mu = 2800$, where u_τ, U_b are the friction and bulk velocity of the channel). The computation domain is $L_x \times L_y \times L_z = 4\pi h \times 2h \times 2\pi h$, where h is the half channel height and x, y, z represents the streamwise, wall normal and spanwise direction, respectively. The corresponding grid points are$N_x \times N_y \times N_z = 225 \times 113 \times 169$ and the resolution in each direction is $\Delta x^+ = 10.1, \Delta z^+ = 6.7$ and $\Delta y^+_{min/max} = 0.2/8.2$. The grid spacing in y-direction is determined by the hyperbolic tangent function $y = -1 + \frac{\tanh(\beta(2y_i - 1))}{\tanh(\beta)}, y_i = (i-1)/(N_y - 1)$, and we chose $\beta = 2.4$ here. Here $(\cdot)^+$ means the variable is normalized by the wall unit. 3-order explicit Euler scheme is used in time and the time step is $dt = 1 \times 10^{-4} (dt^+ = dt \cdot u_\tau/\delta_\nu = 0.00116)$. The computation of channel flow is conducted with constant flow rate method(CFR)[8]. Without other specified, all the variables are normalized by h, U_b in space and velocity field, respectively. The instantaneous velocity is denoted by lower characters, and the ensemble average is denoted by $\overline{u_i}$, where $i = 1, 2, 3$ represents the streamwise, wall normal and spanwise direction, respectively. The fluctuations are represented by $u_i^{'} = u_i - \overline{u_i}$.

Verification of the computation code and the base flow is done firstly by comparing the results of channel flow with $Re_\tau = 180$ from Kim[9](denoted by Kim1987 in the context,see Fig.7). Other statistics also fit the previous numerical and experiments results well, which are not showed here.

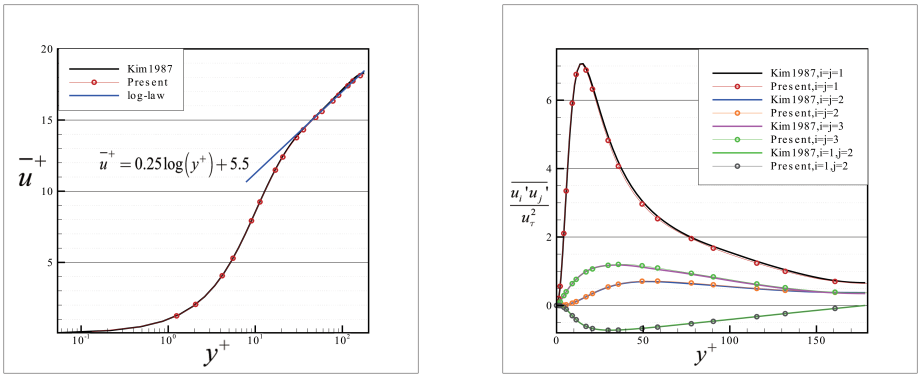

(a) Mean velocity profile (b) Reynolds Stress

Fig. 7. Comparison of the results from our code with Kim1987

Learning from the comparison with the results of Kim1987, we think our computation code can get a satisfied fully developed turbulent channel flow, which is treated as the base flow of our control strategy.

DOI: 10.13009/EUCASS2019-123

2.3 Flow Control

The control strategy, wall blowing and suction of spanwise traveling wave(SpTW-v), $v_w = V_0 \cos(k_z(z - ct))$ is treated as the velocity boundary condition at the wall, where (V_0, k_z, c) is the amplitude, spanwise wavenumber and wave speed traveling wave, respectively. The frequency should be $\omega = k_z c$. The other two components of velocity in streamwise and spanwise direction at the wall are set as no-slip condition ($u_w = w_w = 0$). The sketch of the control is showed in Fig.8. To maintain the symmetry, the top wall is also under control but with a phase difference π, which means $v_w = V_0 \cos(k_z(z - ct) + \pi) = -v_w = -V_0 \cos(k_z(z - ct))$.

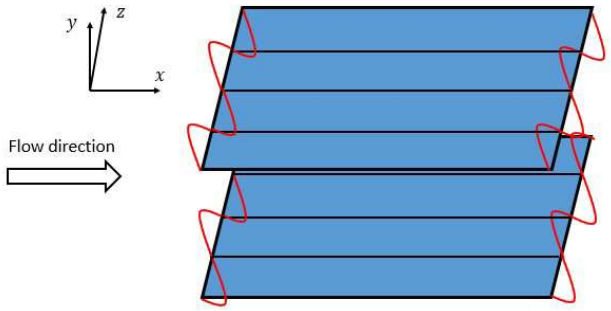

Fig. 8. The sketch of the control in channel flow

Several sets of the parameters are investigated in the context, see Table.1.

The wave speed $c > 0$ in all of the cases, which means the wave of the blowing and suction is traveling along $+z$ direction. Taking the symmetry to consideration, we know the traveling direction of the wave is substantially not vital. In Table.1, the drag reduction efficiency is computed as:

$$DR = \frac{D_{uncontrolled} - D_{controlled}}{D_{uncontrolled}} \times 100\% \tag{25}$$

where $D_{uncontrolled}$ and $D_{controlled}$ are the averaged total drag of both walls without and with control, respectively. Consequently, $DR < 0$ means drag increase and $DR > 0$ means drag reduction. We will focus on Case 8 in what follows.

The first thing is to check the grid independency and computational domain. We use the refined mesh (denoted by Large-RM and the initial mesh is denoted by Large-CM, correspondingly) $N_x \times N_y \times N_z = 225 \times 169 \times 225$ and smaller domain (denoted by Small-RM)with $L_x \times L_y \times L_z = 2\pi h \times 2h \times \pi h$ and its grid resolution $N_x \times N_y \times N_z = 113 \times 169 \times 113$ to simulate the same case as Case 8. Here we only show the grid dependency in Case 8. And also the time step of

DOI: 10.13009/EUCASS2019-123

Table 1. Parameters and drag reduction coefficients in SpTW-v

Case	V_0	k_z	ω	λ^+	T^+	DR
1	0.01	32	32π	35	0.72	1.0%
2	0.1	32	0.2π	35	115	-150%
3	0.1	32	16π	35	1.44	0%
4	0.1	32	32π	35	0.72	0%
5	0.3	12	36	94	2.02	0%
6	0.3	12	16π	94	1.44	0%
7	0.3	16	48	70	1.51	2%
8	0.3	16	16π	70	1.44	2%
9	0.3	32	48	35	1.51	0%
10	0.3	32	16π	35	1.44	2.1%
11	0.3	32	32π	35	0.72	2.1%
12	0.5	16	16π	70	1.44	3.8%
13	0.05	32	0.25π	35	92.6	-75%
14	0.05	32	0.5π	35	46.3	-55%
15	0.05	32	1.6π	35	14.5	-7.5%
16	0.05	32	32π	35	0.72	-2%
17	0.05	24	32π	47	0.72	2.5%
18	0.05	16	32π	70	0.72	2.2%
19	0.05	8	32π	140	0.72	2.2%
20	0.05	32	48π	35	0.48	-2%

DOI: 10.13009/EUCASS2019-123

the case is checked with smaller one, $dt^+ = 0.00115$. The comparison are showed below (Fig.2.3):

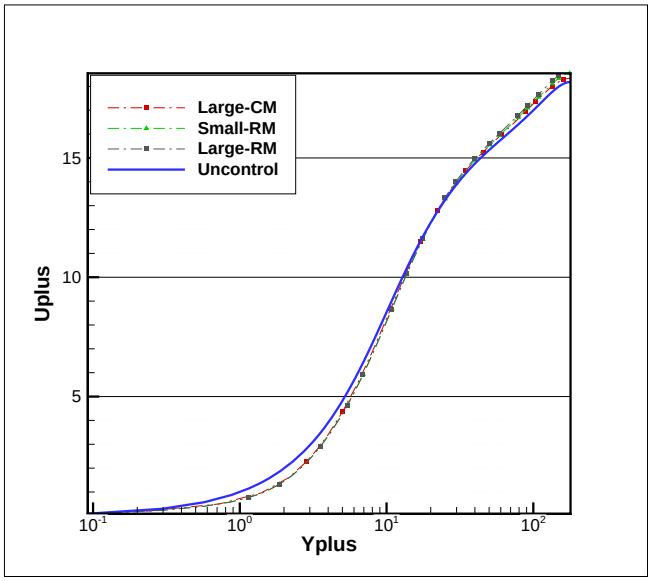

Fig. 9. Mean velocity profile compared with the Large-RM and Small-RM

3 Results and Discussion

3.1 Turbulence Statistics

Since the form of SpTW-v actuation is $v_w = V_0 \cos(k_z(z - ct))$, which is non-homogeneous in spanwise direction and time, we use triple components decomposition[12] here to do statistics to analyze the random fluctuations in the flow. Triple components decomposition method is showed below. For an arbitrary variable (such as $a(x, y, z, t)$) in such flow, it is decomposed to 3 parts:

$$\begin{aligned} a(x, y, z, t) = &\quad \langle a \rangle (y, \phi_z) + a^{''}(x, y, z, t) \\ &= \overline{a}(y) + \tilde{a}(y, \phi_z) + a^{''}(x, y, z, t) \\ &= \quad \overline{a}(y) + a^{'}(x, y, z, t) \end{aligned} \tag{26}$$

where $\overline{a}(y)$ is the ensemble average, $\langle a \rangle (y, \phi_z)$ is the phase average and $\tilde{a}(y, \phi_z)$ is the difference between the ensemble average and the phase average. The $a^{''}(x, y, z, t)$ is the random fluctuations. For the variable $a(x, y, z, t)$, its phase average is defined as:

$$\langle a \rangle (y, \phi_z) = \frac{1}{N_{\phi_z} N_x N_t} [\sum_{l=1}^{N_x} \sum_{s=1}^{N_t} \sum_{k=1}^{N_{\phi_z}} a(x_l, y, z_k, t_s)] \tag{27}$$

DOI: 10.13009/EUCASS2019-123

where N_x is the number of grid points in streamwise, N_t is the time steps used for statistic and N_{ϕ_z} is the number of points in spanwise direction, which are the phase $\phi_z = k_z(z - ct) - 2n\pi, \phi_z \in [0, 2\pi), n \in Z$. Using this decomposition method, for every variable $a(x, y, z, t)$, we can get the average $\overline{a}(y)$, the periodicly varying part $\tilde{a}(y, \phi_z)$, and the random fluctuation $a^{''}(x, y, z, t)$. For the base flow without control, $\tilde{a}(y, \phi_z) = 0$, which means $a^{''}(x, y, z, t) = a^{'}(x, y, z, t)$.

With such triple components decomposition method, analysis of the Reynolds stress based on ensemble average and phase average is done and a comparison of these 2 averaged Reynolds stress with the uncontrolled flow is showed here.

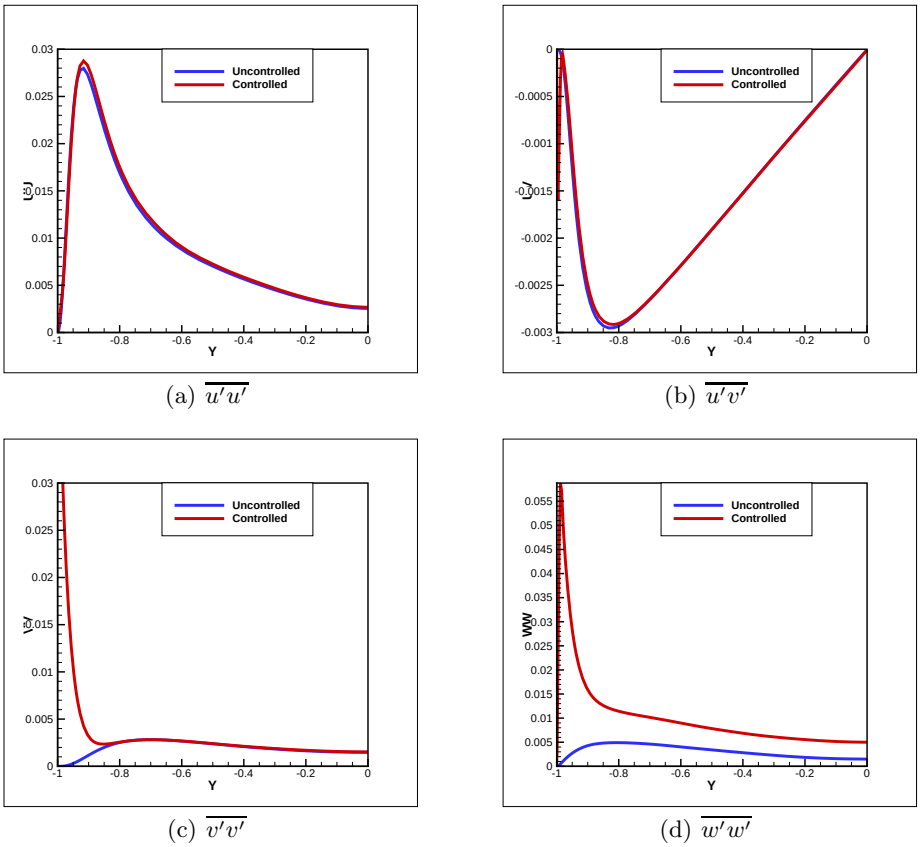

(a) $\overline{u'u'}$ (b) $\overline{u'v'}$

(c) $\overline{v'v'}$ (d) $\overline{w'w'}$

Fig. 10. Comparison of the fluctuations Reynolds stress $\overline{u_i' u_j'}$ with uncontrolled flow

For the results of ensemble average, the mean velocity profile,$\overline{u}^+$, of the controlled flow is larger than that of uncontrolled flow in log-law region, which means SpTW-v leads to a drag reduction by lifting up the viscous layer. But for the Reynolds stress(Fig.10), all the controlled stresses are larger than those

DOI: 10.13009/EUCASS2019-123

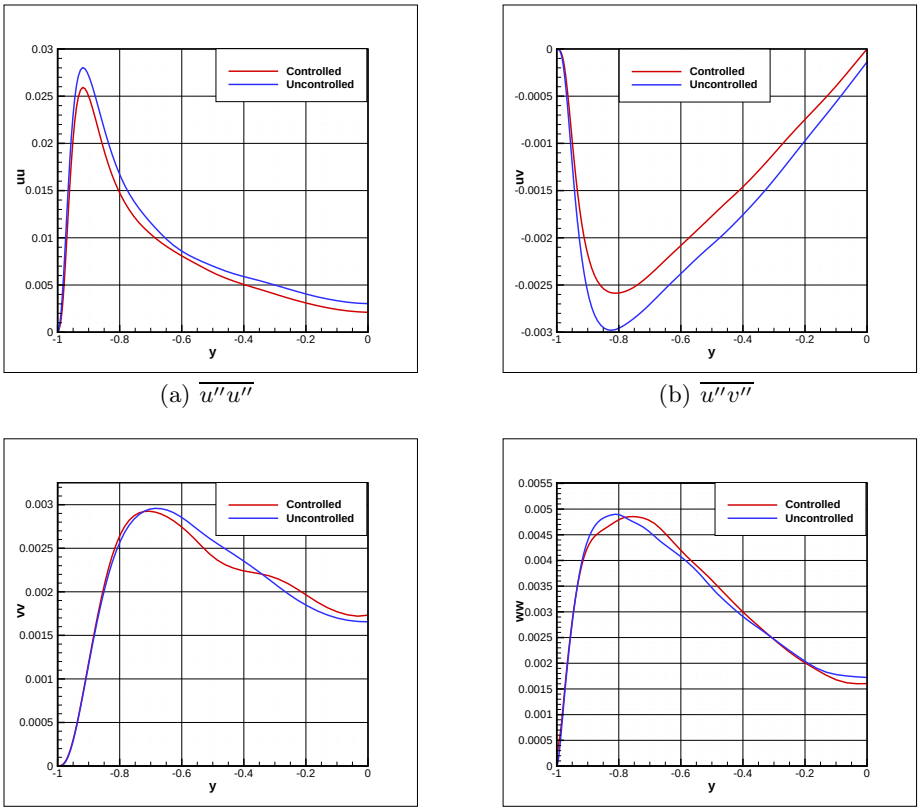

(a) $\overline{u''u''}$ (b) $\overline{u''v''}$

(c) $\overline{v''v''}$ (d) $\overline{w''w''}$

Fig. 11. Comparison of the fluctuations Reynolds stress $\overline{u_i''u_j''}$ with uncontrolled flow

DOI: 10.13009/EUCASS2019-123

in the base flow, especially in $\overline{v'v'}$ and $\overline{w'w'}$, which are far outweigh than the uncontrolled case. Because the wall blowing and suction v_w, whose ensemble average is zero, the induced $v^{'}, w^{'}$ velocity have a periodically varying part and are not purely random. It is these periodically varying parts that lead to a larger Reynolds stress. This is also why we use the triple components decomposition to get the random fluctuations part.

Learning from the Fig.11, we know the phase averaged the shear stress $\overline{u''v''}$ and the streamwise normal stress $\overline{u''u''}$ are obviously smaller than those in uncontrolled flow. For other normal stress, $\overline{v''v''}$ and $\overline{w''w''}$, they are close to the stress in base flow. These results imply that the SpTW-v control reduce the streamwise turbulent fluctuations and thus the friction drag.

3.2 Near Streaks Modification

Here we show the results of comparison of the controlled and uncontrolled in instantaneous turbulent field at some time steps to see how the actuation affect the turbulent structures in turbulent channel. Firstly, the streawise velocity streaks are compared below in Fig.12.

For the streamwise velocity streaks, the actuation inclines the streaks near the wall and the effect can even exist in log-law region. The mechanism behind this inclination effect is similar to that in wall oscillation control. L. Michael et al[13] have studied the inclination of streaks flow control of wall oscillation and concluded that the inclination direction is closely related to the shear strain $(\frac{\partial u}{\partial y}, \frac{\partial w}{\partial y})$, not the wall oscillation velocity or local spanwise velocity directly . As in Fig.13, at this time, the averaged spanwise velocity induced by wall blowing and suction is positive, $w > 0$, but the streaks are inclined to $-z$ direction or say $\theta < 0$. This means the inclination is not related to local spanwise velocity directly. But for the shear strain, $\frac{\partial u}{\partial y} > 0$ and $\frac{\partial w}{\partial y} < 0$, the shear strain $(\frac{\partial u}{\partial y}, \frac{\partial w}{\partial y})$ is close to the inclination direction. The spanwise velocity w induced by the wall blowing and suction v_w with the wave speed $c < 0$, which means the wave is traveling along $-z$ direction has a positive flux. In Fig.13, the averaged spanwise velocity $\overline{w}$ is mostly positive in the whole channel gives a certification to this point. Also in the profile of the $\overline{w}$, from the location $y = -0.4(y^+ = 72)$,the derivative $\frac{\partial w}{\partial y} \approx 0$, means the inclination angle should close to 0, which is true in the results.

3.3 Conditional Average

To investigate how the actuation affect the streamwise vortex in the flow, we use the method named conditional average. The process of conditional average is that firstly select an xz-plane at a wall normal location, such as $y^+ = 20$. Then detect the vortex cores at this plane. The vortex core criterion used here is the extreme points of Q value. When finding a vortex core, get the sign of the streamwise vorticity. ω_x. Take all the vortex core having the same sign of streamwise vorticity to the same location, such as $(y^+, z^+) = (20, 0)$. Then do average of the all the flow variables in the regions near these vortex cores. In one word, the conditional

DOI: 10.13009/EUCASS2019-123

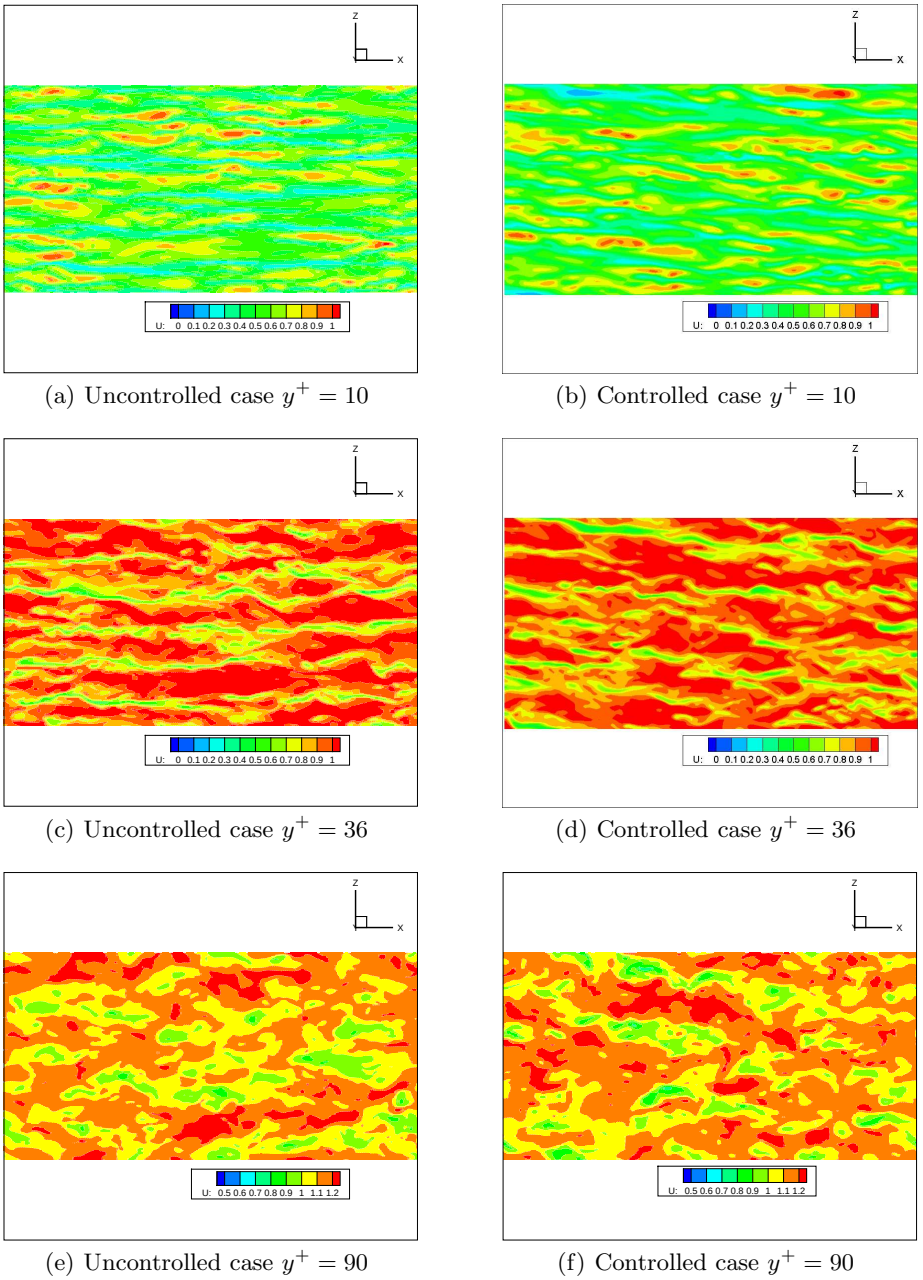

(a) Uncontrolled case $y^+ = 10$ (b) Controlled case $y^+ = 10$

(c) Uncontrolled case $y^+ = 36$ (d) Controlled case $y^+ = 36$

(e) Uncontrolled case $y^+ = 90$ (f) Controlled case $y^+ = 90$

Fig. 12. Comparison of the fluctuations Reynolds stress $\overline{u_i'' u_j''}$ with uncontrolled flow

DOI: 10.13009/EUCASS2019-123

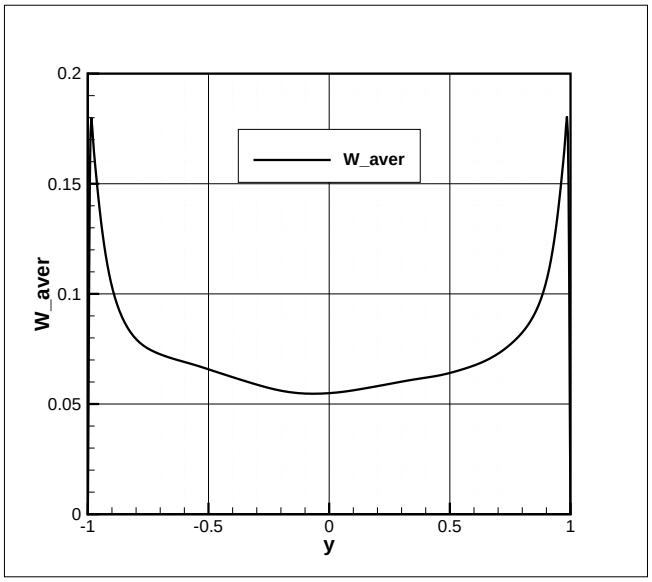

Fig. 13. The average spanwise velocity at one time step

average is using one vortice to represent all the vortex with the same rotation direction at one xz-plane. Using this method, we can know the average affect of the SpTW-v actuation to the streamwise vortex at some y^+ location.The results are showed below. In Fig.14,Fig.15, which shows the conditional averaged flow field with positive and negative ω_x, respectively,the vector $(w^{''}, v^{''})$ shows the rotation of the vortex and the contour shows the range of the streamwise fluctuations u''. The $u'' > 0$ means burst events and the $u'' < 0$ means sweep events, which are important to the self-maintenance of the streamwise vortex in turbulent channel. The solid lines in these figures (Fig.14,Fig.15) shows the location of the vortex core. Of course, with mentioned process of the conditional average , the vortex cores are moved to $(y^+, z^+) = (20, 0)$.

As shown in the results of conditional average, SpTW-v actuation has different effects to the streamwise vortex of different signs. For vortex with $\omega_x > 0$, SpTW-v actuation weaken the burst events of these vortex slightly and for vortex with $\omega_x < 0$, SpTW-v actuation has stronger effects and the burst and sweep events are both weakened and thus the drag is reduced.

3.4 Energy consideration

In this section, we will evaluate this control strategy in energy consumption aspects. The pumping work for the channel is:

$$W_p = -\overline{\frac{dP}{dx}} U_b \tag{28}$$

DOI: 10.13009/EUCASS2019-123

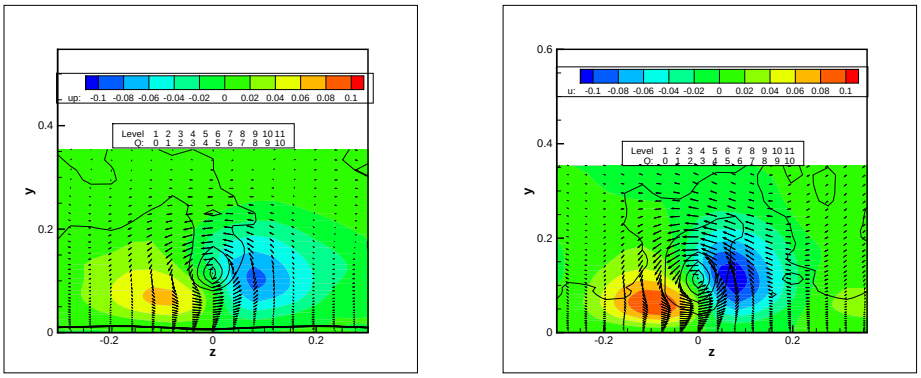

(a) Controlled (b) Uncontrolled

Fig. 14. The conditional averaged flow field around the vortex cores with negative streamwise vorticity

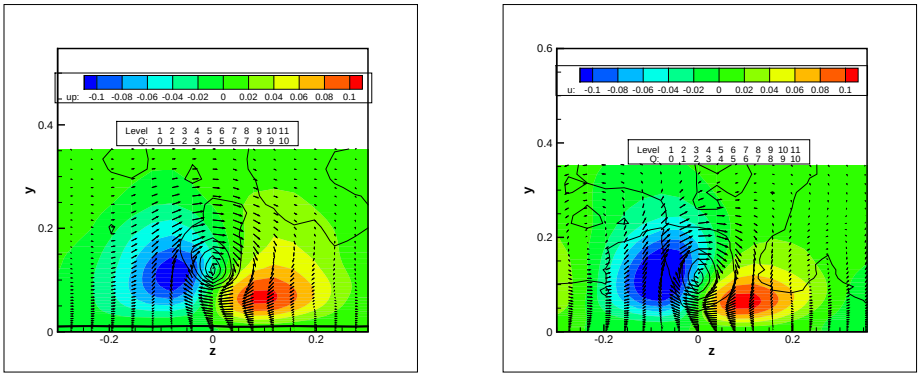

(a) Controlled (b) Uncontrolled

Fig. 15. The conditional averaged flow field around the vortex cores with positive streamwise vorticity

DOI: 10.13009/EUCASS2019-123

where $\overline{\frac{dP}{dx}}$ is the average pressure drop in streamwise direction and U_b is the bulk velocity of the channel. The actuation work of the control is:

$$W_a = \frac{2}{L_x L_z} \int_0^{L_x} \int_0^{L_z} (p_w + \frac{1}{2} v_w^2) v_w dx dz \tag{29}$$

where p_w, v_w mean the pressure and velocity in wall normal direction at the wall, and the factor "2" collects the energy of both walls. Then the energy gain rate G and net save rate S are:

$$G = \frac{W_{p0} - W_p}{W_a} \tag{30}$$

$$S = \frac{W_{p0} - (W_p + W_a)}{W_{p0}} \tag{31}$$

where W_{p0} is the pumping power of the uncontrolled case. In Case 8, we find the energy input is $W_a = 0.1414$, and the pumping power of the uncontrolled flow is $W_{p0} = 0.326$. Since the drag reduction is 2.2%, the pumping power of the actuated flow is $W_p = 0.319$. Then we know, the actuation cost about 43% power of the flow but save only 2% of the drag, which leads to a net energy save $S = -41\%$. This control strategy may not be a energy saving one.

3.5 Linearized Fluctuations Analysis

We will analyze the drag reduction mechanism of the SpTW-v actuation in this section. From the previous results of the turbulent statistics and instantaneous flow field, the SpTW-v can weaken the burst and sweep events of the streamwise vortex and the streamwise fluctuations and thus leads to drag reduction. To understand the mechanism, we use the linearized fluctuations equation based on incompressible laminar channel flow as the base flow to see how the actuation affect the base flow. The incompressible NS equations:

$$\frac{\partial \underline{u}}{\partial t} + \underline{u} \bullet \nabla \underline{u} = -\frac{1}{\rho} \nabla p + \nu \nabla^2 \underline{u} \tag{32}$$

$$\nabla \bullet \underline{u} = 0 \tag{33}$$

where $\underline{u} = [u, v, w]^T$ is the velocity vector. For the laminar channel flow, only the streamwise velocity is non-zero and dependent only on y. In other words, the canonical flow is: $u = U(y) = U_c(1 - y^2), v = w = 0$, and the actuated flow equations:

$$\frac{\partial (\underline{u + u'})}{\partial t} + (\underline{u + u'}) \bullet \nabla (\underline{u + u'}) = -\frac{1}{\rho} \nabla (p + p') + \nu \nabla^2 (\underline{u + u'}) \tag{34}$$

$$\nabla \bullet (\underline{u + u'}) = 0 \tag{35}$$

and the boundary conditions are: $v'|_{y=\pm 1} = \mp V_0 \cos(k_z(z - ct)), u'|_{y=\pm 1} = w'|_{y=\pm 1} = 0$. Linearize the above equations, and the homogeneity in stream-

DOI: 10.13009/EUCASS2019-123

wise direction, $\frac{\partial}{\partial x} = 0$.

$$\frac{\partial u'}{\partial t} + v'\frac{\partial U}{\partial y} = -\frac{1}{\rho}\frac{\partial p'}{\partial x} + \nu(\frac{\partial^2 u'}{\partial y^2} + \frac{\partial^2 u'}{\partial z^2}) \tag{36}$$

$$\frac{\partial v'}{\partial t} = -\frac{1}{\rho}\frac{\partial p'}{\partial y} + \nu(\frac{\partial^2 v'}{\partial y^2} + \frac{\partial^2 v'}{\partial z^2}) \tag{37}$$

$$\frac{\partial w'}{\partial t} = -\frac{1}{\rho}\frac{\partial p'}{\partial z} + \nu(\frac{\partial^2 w'}{\partial y^2} + \frac{\partial^2 w'}{\partial z^2}) \tag{38}$$

$$\tag{39}$$

where $[u', v', w', p']^T$ represents the streamwise, wall normal, spanwise and pressure fluctuations, respectively. Note the equations of (v', w', p') are closed and we can solve the equations of (v', w', p') and then solve the u' equation. As mentioned above, we have got the linearized solution of the induced flow by this actuation in a half-infinite field (Eq.18)and the same methods can be used to get the corresponding solution in channel flow case, or see Ref.**??**. For Case 8, $k_z = 16$, the results of different frequency ω are showed below:

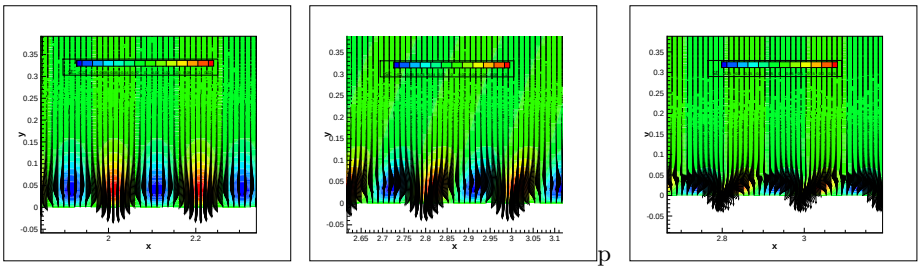

(a) $\omega = 8.92 \times 10^{-4}$ (b) $\omega = 8.92 \times 10^{-2}$ (c) $\omega = 16$

Fig. 16. The streamwise fluctuations induced by the SpTW-v

From the results, when ω is close to 0, in other words, the wall blowing and suction actuation is almost steady, u' is positive above the suction region and u' is negative above the blowing region. As we know, close to the wall, $u' > 0$ means the streamwise velocity increases and thus drag increases. In contrast, $u' < 0$ means the streamwise velocity decreases and the drag reduces. When the wave speed or frequency is small enough, low speed flow are lifted above the blowing region and the high speed flow are pulled down above the suction region, since the only production term in streamwise fluctuation equation is $v'\frac{\partial U}{\partial y}$. Thus, there is drag increase near the suction region and drag reduction near the blowing region. When ω gets larger, or the wave speed is larger, the $u' > 0$ parts move to the forward region and also $u' < 0$ move to the backward region. When the frequency $\omega = 16$, the forward region almost coincides with the $u' > 0$ region and the backward region coincides with the $u' < 0$ region.

DOI: 10.13009/EUCASS2019-123

Although these results are gotten from laminar base flow, there are some interesting conclusions related to the drag reduction mechanism behind the SpTW-v control. Learning from the linearized fluctuations equations, we know the backward region coincides with drag reduction region and the forward region coincides with drag increase region. With the analysis in former sections, the forward region shrinks and backward region expands when wave speed or frequency increases, which also means the drag reduction region expands and drag increase region shrinks. For example in other cases, the frequency is getting larger, $\omega = 0.25, 0.5, 1.6, 16, 32, 48...$, and thus the drag reduction efficiency is getting larger. On the other hand, the amplitude affect the range of the streamwise fluctuations u', obviously, which also means the extent of drag reduction or increase. The comparison of others also shows this point with larger drag reduction when the frequency is larger. Also, $u' < 0$ means smaller turbulent fluctuations and $u' > 0$ means larger turbulent fluctuations. When $u' < 0$ regions get larger and $u' < 0$ get smaller, the streamwise fluctuations are restrained and thus streamwise normal stress and shear stress.

4 Alternating traveling wave

As mentioned above, the traveling of blowing and suction actuation will induce a flux opposite to the wave propagation direction and this might lead to spanwise flux. The drag reduction rate of this control pattern seems very limited because of the spanwise motion near the center of the channel. In order to weaken this spanwise motion, we use alternating traveling wave, which means the direction of wavespeed is changed alternately or in other words, the propagation direction of the wave is changed. With this modification to the original traveling wave strategy, we achieve a larger drag reduction rate. The details of the actuation is:

$$v_w = V_0 \cos(k_z(z - ct)), t < T_a \tag{40}$$

$$v_w = V_0 \cos(k_z(z + ct) + \phi_0), T_a < t < 2T_a \tag{41}$$

where T_a is the time for traveling wave in one direction and ϕ_0 is the phase

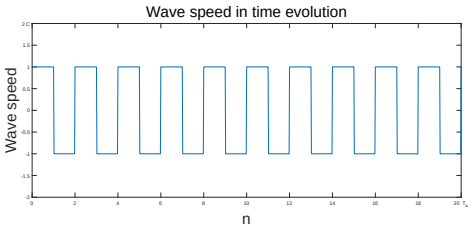

Fig. 17. Wave speed at different time

difference to ensure continuity. Intuitively, the wave is traveling in $+z$ direction

DOI: 10.13009/EUCASS2019-123

during $0 < t < T_a$, then traveling back in $T_a < t < 2T_a$. The same techniques used above will be also used to analysis the flow here with the alternating traveling wave. For the mean velocity profile compared to the uncontrolled case (Fig.18), we can see the line is lifted up a lot in log-law region, which means a large drag reduction. In fact, we achieve a 30% drag reduction with the parameters $(V_0, k_z, c, T_a) = (0.3, 16, \pi, 10)$ or normalized by wall units $(V_0^+, \lambda_z^+, c^+, T_a^+) = (4.67, 79.7, 48, 8, 115.7)$. The phase average of the flow field

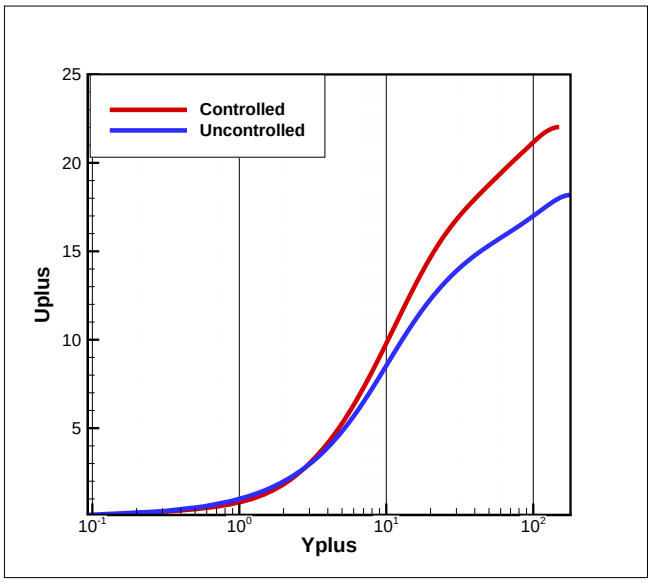

Fig. 18. Mean velocity profile with $(V_0, k_z, c, T_a = (0.3, 16, \pi, 10))$

now need to be separated to 2 parts, $c > 0$ and $c < 0$. Ignoring the transient part near the change of the wavespeed, we only consider the flow at the "steady" state. In the post-process, we only analysis the data at the time $t = T_a - 1$ near the end of each period $T_a, 2T_a$. From the phase averaged Reynolds stress (Fig.19), we learn that the random fluctuations are weakened much and thus the drag. And there is few difference between the phase average in CP and CN periods. So in the following, we consider the CP periods only. As for the near-wall streaks, similar to one-direction traveling wave, in each periods, the streaks are inclined and also elongated (Fig.20).

5 Conclusion

The control strategy of the spanwise traveling wave of wall blowing and suction(SpTW-v),$v_w = V_0 \cos(k_z(z - ct))$ and its effect to drag reduction are investigated here.

DOI: 10.13009/EUCASS2019-123

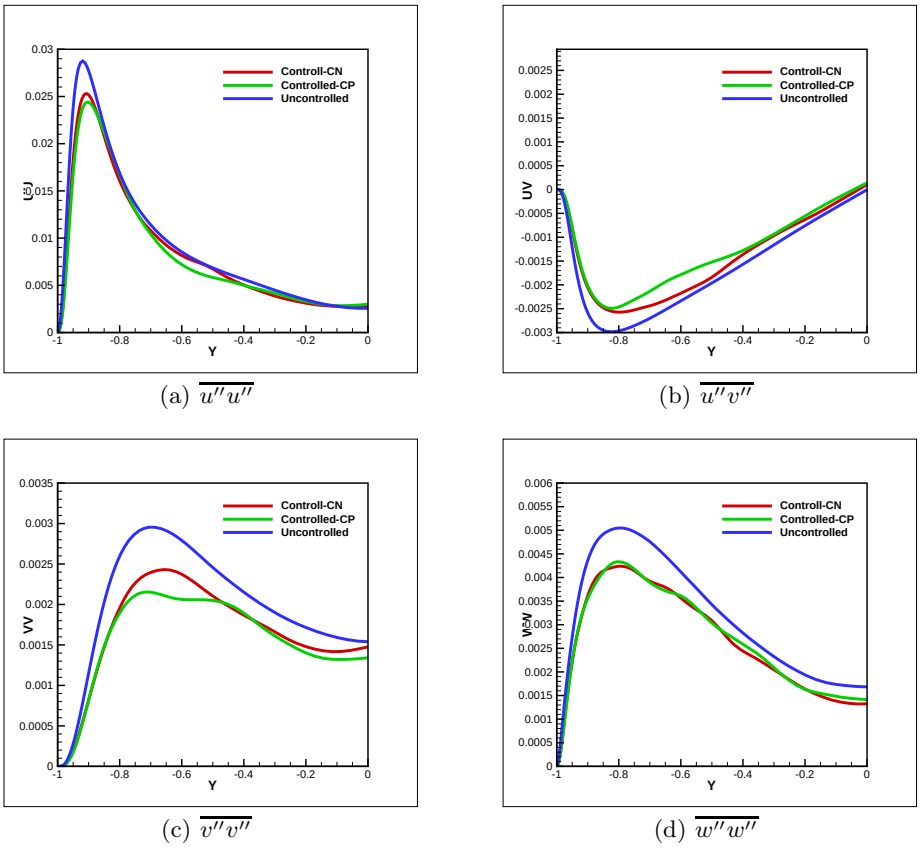

(a) $\overline{u''u''}$ (b) $\overline{u''v''}$

(c) $\overline{v''v''}$ (d) $\overline{w''w''}$

Fig. 19. Comparison of the fluctuations Reynolds stress $\overline{u_i'' u_j''}$ in CP($c > 0$) and CN($c < 0$)with uncontrolled flow

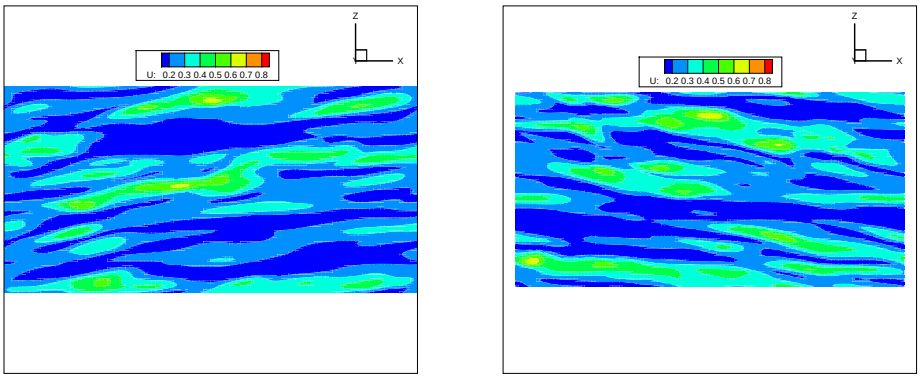

(a) CP (b) CN

Fig. 20. The streamwise velocity streaks in CP and CN periods at $y^+ = 5.4$

DOI: 10.13009/EUCASS2019-123

Unlike other active control, we get relatively smaller drag reduction with this control method. With the parameters $(V_0, k_z, c) = (0.3, 16, -\pi)$, we have a drag reduction about 2%. From the results of fluctuations analysis, wall blowing and suction forms drag increase region and reduction region, and in another aspect, backward region and forward region. When the blowing and suction are traveling along spanwise direction,backward region gets closer to drag reduction region and forward region gets closer to drag increase region. When the wavespeed or frequency is larger enough, drag reduction region coincides with the forward region and increase region coincides with backward region. At the same time, the drag increase region and forward region get smaller and reduction region and backward region get larger. As a results the streamwise fluctuations are restrained and thus the normal stress $\overline{u''u''}$ and shear stress $\overline{u''v''}$. In addition, the burst and sweep events of the near wall streamwise vortex are inhibited by the SpTW-v actuations. On the other hand, the spanwise motion induced by SpTW-v actuations make the near wall streaks inclined, affects the turbulent structures. From the analysis of our work, in order to get higher drag reduction efficiency, the wave speed c or frequency ω can be chosen larger to make the drag increase region or forward region smaller. When making the direction of wave traveling is alternating, we can achieve a much higher drag reduction about 30%. The mechanism behind this strategy needs more consideration.

References

1. Choi, H., Moin, P., Kim J. : Direct numerical simulation of turbulent channel flow over riblets. J. Fluid. Mech. 255?503 (1993)
2. Quardrio, M., Pierre, R. : Initial response of a turbulent channel flow to spanwise oscillation of the walls. Journal of Turbulence. 4:N7 (2003)
3. Quardrio, M., Pierre, R. : Critical assessment of turbulent drag reduction through spanwise wall oscillation. J. Fluid. Mech. 521, 251?271 (2004)
4. Quadrio, M., Pierre, R. : Streamwise-traveling waves of spanwise wall velocity for turbulent drag reduction. J. Fluid. Mech. 627, 161 (2009)
5. Min, T., Kang, S.M., Speyer J.L., John, K. : Sustained sub-laminar drag in a fully developed channel flow. J. Fluid. Mech. 558, 309 (2006)
6. Tomiyama, N., Fukagata, K. : Direct numerical simulation of drag reduction in a turbulent channel flow using spanwise traveling wave-like wall deformation. Physics of Fluid. 105?115 (2013)
7. Gao, H., Wang, Z. : A conservative correction procedure via reconstruction formation with the chain-rules divergence evaluation. Journal of Computational Physics. 232(1), 7?13 (2013)
8. Lenormand, E., Sagua, P., Ta Phuoc, L. : Large eddy simulation of subsonic and supersonic channel flow at moderate Reynolds number. International Journal for numerical methods in Fluids. 32, 369?406 (2000)
9. Kim, J., Moin, P., Moser, R. : Turbulence statistics in fully developed channel flow at low Reynolds number. J. Fluid. Mech. 177, 133?166 (1987)
10. Hoeffner, J., Fukagata, K. : Pumping or drag reduction?. J. Fluid. Mech. 635, 171?187 (2009)
11. Woodcock, J.D., Sader, J., Marusic, I. : Induced flow due to blowing and suction flow control: an analysis of transpiration. J. Fluid. Mech. 690, 366?398 (2012)

DOI: 10.13009/EUCASS2019-123

12. Reynolds, W.C., Hussain, A.K.M.F. : The mechanics of an organized wave in turbulent shear flow. 54, 263?288 (1972)
13. Touber, E., Michael, A.L. : Near-wall streak modification by spanwise oscillatory wall motion and drag-reduction mechanism. J. Fluid. Mech. 693, 150?200 (2012)